Hydroxylamine Complexes of Cytochrome *c′*: Influence of Heme Iron Redox State on Kinetic and Spectroscopic Properties

Brianna N. Brown,[†] Kelsey J. Robinson,[†] Quentin C. Durfee,[†] Demet Kekilli,[‡,//], Michael A. Hough,[‡] Colin R. Andrew[*,†]*

[†]Department of Chemistry and Biochemistry, Eastern Oregon University, La Grande OR 97850, United States

[‡]School of Life Sciences, University of Essex, Wivenhoe Park, Colchester Essex, CO4 3SQ, UK

ABSTRACT: Hydroxylamine (NH_2OH or HA) is a redox-active nitrogen oxide that occurs as a toxic intermediate in the oxidation of ammonium by nitrifying and methanotrophic bacteria. Within ammonium containing environments, HA is generated by ammonia monooxygenase (nitrifiers) or methane monooxygenase (methanotrophs). Subsequent oxidation of HA is catalyzed by heme proteins, including cytochromes P460 and multi-heme hydroxylamine oxidoreductases, the former contributing to emissions of N_2O, an ozone-depleting greenhouse gas. A heme-HA complex is also a proposed intermediate in the reduction of nitrite to ammonia by cytochrome *c* nitrite reductase. Despite the importance of heme-HA complexes within the biogeochemical

nitrogen cycle, fundamental aspects of their coordination chemistry remain unknown, including the effect of Fe redox state on heme-HA affinity, kinetics, and spectroscopy. Using stopped-flow UV-vis and resonance Raman spectroscopy, we investigated HA complexes of the L16G distal pocket variant of *Alcaligenes xylosoxidans* cytochrome *c'*-α (L16G AxCP-α), a pentacoordinate *c*-type cytochrome that we show binds HA in its Fe(III) (K_d ~ 2.5 mM) and Fe(II) (K_d = 0.0345 mM) states. The ~70-fold higher HA affinity of the Fe(II) state is due mostly to its lower k_{off} value (0.0994 s^{-1} vs 11 s^{-1}), whereas k_{on} values for Fe(II) (2,880 M^{-1} s^{-1}) and Fe(III) (4,300 M^{-1} s^{-1}) redox states are relatively similar. A comparison of the HA and imidazole affinities of L16G AxCP-α was also used to predict the influence of Fe redox state on HA binding to other proteins. Although HA complexes of L16G AxCP-α decompose via redox reactions, the lifetime of the Fe(II)HA complex was prolonged in the presence of excess reductant. Spectroscopic parameters determined for the Fe(II)HA complex include the N–O stretching vibration of the NH_2OH ligand, ν(N–O) = 906 cm^{-1}. Overall, the kinetic trends and spectroscopic benchmarks from this study provide a foundation for future investigations of heme-HA reaction mechanisms.

INTRODUCTION

Hydroxylamine (NH_2OH or HA) is a redox-active intermediate in the global biogeochemical nitrogen cycle, whose metabolism is integral to microbial energy transduction and the interconversion of agriculturally and environmentally important nitrogen species.[1,2] Within ammonium-rich environments (*e.g.* wastewater treatment plants and fertilized fields), the exergonic nitrification pathway begins with the formation of HA from ammonium, catalyzed by

ammonia monooxygenase (nitrifying bacteria),[3] or methane monooxygenase (methanotrophs).[4,5] Subsequent oxidation of the energy-rich (but toxic) HA species is catalyzed by heme enzymes, including cytochrome P460 and hydroxylamine oxidoreductase (HAO), both of which convert HA to an initial heme-bound nitric oxide (NO) species that can be further oxidized via additional enzymatic and/or non-enzymatic activity. In the case of *Nitrosomonas europaea* cytochrome P460 (NeP460), heme-bound NO reacts with an additional HA molecule under anaerobic conditions to form N_2O (an ozone-depleting greenhouse gas),[1, 6] whereas aerobic conditions lead to the release of NO followed by its non-enzymatic oxidation to NO_2^-.[1] In addition to the role of heme cofactors in HA oxidation, a heme-HA complex is a proposed intermediate in the six-electron reduction of nitrite to ammonia catalyzed by cytochrome *c* nitrite reductase, which enables certain bacteria to utilize nitrite as a terminal electron acceptor.[7,8] The ability of cytochrome *c* nitrite reductase to reduce HA may also function to protect bacteria from HA toxicity.[9] It has also been postulated that the ability of non-symbiotic plant hemoglobins (phytoglobins) to reduce HA might be physiologically relevant during hypoxic metabolism.[10,11]

Scheme 1. Reversible Binding of Hydroxylamine to Heme.

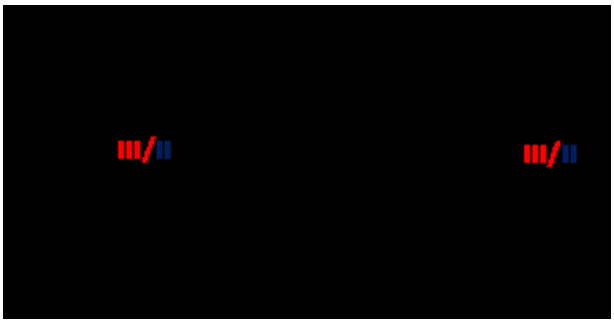

Hydroxylamine binding (k_{on}) and release (k_{off}) can occur with the heme cofactor in its Fe(III) or Fe(II) redox state. Endogenous and solvent axial ligands have been omitted for clarity.

As the conjugate base of hydroxylammonium, $^{+}NH_3OH$ (pK_a 5.96),[12] neutral NH_2OH is able to bind to heme Fe in both its Fe(III) or Fe(II) forms (Scheme 1), and indeed, both redox states may contribute to mechanisms of heme-HA metabolism. However, the influence of Fe redox state on heme-HA coordination (including its effect on HA affinity and rate constants for HA binding, k_{on}, and release, k_{off}) has not been reported, presumably due to the rapid decomposition exhibited by many iron HA complexes. Some stable heme protein Fe(III)HA species have been reported in truncated rat heme oxygenase,[13] *Arthromyces ramosus* peroxidase,[14,15] N-acetylmicroperoxidase-8,[16] *Wolinella succinogenes* cytochrome *c* nitrite reductase,[7] and cytochromes P460 from *Nitrosomonas europaea* (NeP460),[1] and *Nitrosomonas sp.* AL212 (AL212P460).[17,18] However, many Fe(III) porphyrins (including hemoglobin) undergo reduction to the Fe(II) state without an observable Fe(III)HA intermediate, accompanied by the formation of a range of nitrogenous end products, including NO, N_2O, N_2, or NH_4^+.[19-23] Conversely, studies of heme proteins in their Fe(II) state have shown that HA oxidizes the heme to Fe(III) with the subsequent formation of NH_4^+.[11,24,25] Although an Fe(II)HA complex is a proposed intermediate in this process, the only heme protein Fe(II)HA complex observed to date is a transient species in stopped-flow studies of HA reactivity with the distal H73L variant of rice phytoglobin.[24] A transient complex (λ_{max} 663 nm) was also recently reported during the oxidation of Fe(II) NeP460 by HA.[1] Within model porphyrins, observed Fe(II)HA complexes include an Fe(II)$(HA)_2$ species formed with Fe(II)TPP (TPP = tetraphenylporphyrin) at low temperature,[19] and an Fe(II)HA complex generated from the three electron reduction of Fe(II)(OEP)NO (OEP = octaethylporphyrin) in the presence of weak organic acids.[26,27]

Cytochromes *c′* are NO-binding heme proteins found in photosynthetic, methanotrophic, denitrifying, sulfur-oxidizing, and nitrogen fixing organisms, that have proposed roles in

protecting bacteria from nitrosative stress.[28] Typically homodimeric, cytochromes *c′* contain a pentacoordinate CXXCH *c*-heme-binding motif located close to the C-terminus. Two distinct and unrelated types of cytochrome *c′* have been identified, designated cytochrome *c′*-α or cytochrome *c′*-β according to their secondary structure.[27-30] Within the cytochrome c′-α family, exogenous ligand binding to the distal heme site is hindered by an occluding hydrophobic residue (most often Leu, but sometimes Phe, Tyr or Met)[28]. Extensive characterization of *Alcaligenes xylosoxidans* cytochrome *c′*-α (AxCP-α) has shown that replacement of the occluding Leu16 with smaller residues dramatically boosts ligand binding affinity.[32-34] In particular, the L16A variant exhibits ultrahigh Fe(II) heme affinities for diatomic gases: NO (K_d ~ 70 fM), CO (K_d ~ 3.4 pM), O_2 (K_d ~ 49 nm).[33] The related L16G variant of AxCP-α also binds gases with high affinity, as exemplified by the Fe(II)CO complex (K_d ~ 15 pM).[32] Most recently, the relatively high nitrite affinity of the L16G AxCP-α variant was used by us to characterize NO_2^- coordination to Fe(III) heme, including the use of vibrational spectroscopy to distinguish N- vs O-bound isomers.[35]

In this study, we utilized the enhanced distal heme reactivity of the L16G AxCP-α variant to characterize its Fe(III)HA and Fe(II)HA complexes. Our time-resolved UV-vis absorption measurements reveal the influence of heme redox state on heme-HA affinity, including the rate constants for HA binding and release. Using resonance Raman (RR) spectroscopy, we also identify the N–O stretching vibration of the NH_2OH ligand, providing a spectroscopic handle for future studies of heme-HA reaction mechanisms.

EXPERIMENTAL SECTION

Protein Samples and Reagents. The L16G variant of AxCP-α was expressed and purified as previously described.[32] Conversion of the as-isolated Fe(II)CO form of L16G AxCP-α to the

Fe(III) state was achieved by reacting with 0.8 M ferricyanide (final concentration) for 10 min,[32] followed by removal of oxidant with a P6-DG column. Sodium dithionite was used to reduce Fe(III) protein to the Fe(II) state. Hydroxylamine hydrochloride, including isotopically labelled $^{15}NH_2OH.HCl$, (98% ^{15}N, 99% CP), was obtained from Sigma-Aldrich. The concentrations of anaerobic HA stock solutions (~1.0 M) were calculated from the dry weight of $NH_2OH.HCl$ dissolved in deionized water inside a glove box (<1 ppm O_2). Final concentrations of reagents and protein samples used in kinetic and spectroscopic measurements of heme-HA complexes were prepared in pH 8.0 buffer containing 50 mM HEPES and 0.10 M NaCl. Corresponding kinetics measurements of heme-imidazole complexes were conducted in pH 8.9 buffer containing 50 mM CHES and 0.10 M NaCl.

Spectroscopic Measurements. UV-vis absorption spectra of L16G AxCP-α solutions (~5 μM in heme), housed within anaerobic septum-sealed quartz cuvettes, were measured at 25.0 °C using a Cary 60 scanning spectrophotometer with a temperature-controlled cell holder. Raman and resonance Raman (RR) measurements were performed at room temperature on anaerobic samples contained within septum-sealed glass capillary tubes. Spectra were recorded using a custom McPherson 2061/207 spectrograph equipped with a Princeton Instruments liquid N_2-cooled (LN1100PB) CCD detector. Spectral dispersal was achieved using a 0.67 m focal length and 2400 grooves/mm holographic grating. An excitation wavelength of 406.7 nm was provided by a Kr ion laser, and the Rayleigh line was attenuated using a long-pass filter (RazorEdge, Semrock). Spectra were measured over periods of 1 – 2 mins using 16 mW laser power at the sample and a 90° scattering geometry, with Raman shifts calibrated to an accuracy of ± 1 cm^{-1} using an indene standard. RR measurements of L16G AxCP-α were conducted on samples containing ~150 μM protein (in heme). A modified Cary 50 UV-visible spectrophotometer was used to confirm the

integrity of heme complexes before and after RR data collection. Raman spectra of non-complexed hydroxylamine in its acid (pH 3.5) and conjugate base (pH 8.0) forms were measured using 0.5 M solutions of $NH_2OH.HCl$ dissolved in water, with the pH adjusted as required with $NaOH_{(aq)}$.

Kinetics Measurements. Time-resolved absorbance measurements were performed anaerobically at 25.0 °C using either an Applied Photophysics SX.18MV-R stopped-flow spectrophotometer housed within a Vacuum Atmospheres glove box, or a Cary 60 UV-visible absorbance spectrophotometer. To ensure the stability of the Fe(II) redox state, kinetic measurements of HA and Im binding to Fe(II) L16G AxCP-α were conducted in the presence of ~ 0.1 mM sodium dithionite (it was determined that dithionite did not react with HA or Im). The k_{on} value for the Fe(II)HA complex was determined using stopped-flow kinetics by reacting Fe(II) L16G AxCP-α with 50 – 800 μM HA (after mixing) and monitoring changes in UV-visible absorbance using either a photodiode array (PDA) or photomultiplier tube (PMT) detector. Time courses at 413 nm (λ_{max} of the Fe(II)HA complex) were fitted with a single exponential function to yield k_{obs} values. A plot of k_{obs} vs [HA] yielded the k_{on} value from the slope of a linear fit. The k_{off} value for the Fe(II)HA complex was determined in separate ligand replacement experiments with CO (which binds rapidly to Fe(II) L16G AxCP-α).[32] Upon mixing with CO (0.25 – 0.50 mM after mixing), the resultant Fe(II)HA → Fe(II)CO conversion (with HA release as the rate determining step) was monitored via stopped-flow measurements using a PDA detector, with k_{off} determined from a single exponential fit of the 418 nm absorbance time course. The k_{on} value for the Fe(II)Im complex was measured via stopped-flow spectrophotometry by reacting Fe(II) protein with 50 – 500 μM Im and monitoring changes using a PDA detector. Pseudo first order rate constants (k_{obs}) for Fe(II)Im formation were determined from single exponential fits of 437-nm time courses (corresponding to the disappearance of Fe(II) L16G AxCP-α absorbance). A plot of

k_{obs} vs [Im] yielded the k_{on} value from the slope of a linear fit. The corresponding off-rate constant was measured by mixing the Fe(II)Im complex with 0.5 mM CO, and monitoring the conversion to the Fe(II)CO complex (λ_{max} 418 nm) (with Im release as the rate determining step) using a Cary 60 UV-visible spectrophotometer. A single exponential fit of the 418-nm time course yielded k_{off}.

The bimolecular on-rate constant (k_{on}) for the Fe(III)HA complex was determined by stopped-flow measurements under pseudo first order conditions by reacting Fe(III) L16G AxCP-α with a HA (0.60 – 15 mM after mixing) and monitoring changes in UV-visible absorbance using either a PDA or PMT detector. Pseudo first-order rate constants (k_{obs}) were determined from single exponential fits of absorbance time courses at 409 nm (λ_{max} of the Fe(III)HA complex). The value of k_{on} was obtained from the slope of a plot of k_{obs} vs [HA], with the off-rate constant (k_{off}) determined from the *y*-intercept. The k_{on} value for the Fe(III)Im complex was determined from stopped-flow measurements by reacting Fe(III) L16G AxCP-α with Im (50 – 500 μM after mxing) and monitoring changes in the absorbance at 415 nm using a PMT detector. Values of k_{obs} were determined from single exponential fits of 415-nm time courses. A plot of k_{obs} vs [HA] yielded the k_{on} value from the slope of a linear fit. The k_{off} value for the Fe(III)Im complex was determined in separate ligand replacement experiments with NO using a Cary 60 spectrophotometer. After mixing with 1.0 mM NO, the Fe(III)Im complex converted to the Fe(III)NO species (λ_{max} 418, 536, 567 nm) in a rate-determining step corresponding the release of the Im ligand, after which the Fe(III)NO complex undergoes a slower reductive nitrosylation to the Fe(II)NO species (λ_{max} 416, 541, 572 nm), as previously reported.[35] The k_{off} value for Fe(III)Im complex (corresponding to the rate of Fe(III)NO formation) was obtained from the first phase of a double exponential fit of the 421-nm time course.

Dissociation Constants (K_d). For each of the L16G AxCP-α complexes studied, K_d values were calculated from the ratio of k_{off}/k_{on}. The relatively low ligand affinity of the Fe(III)HA complex also enabled its K_d value to be determined via titration from stopped-flow measurements under non-saturating HA concentrations. In this case, the amplitude of each 409 nm time course (ΔA_{409}) (corresponding to Fe(III)HA formation) was plotted vs HA concentration ([HA]) to generate an HA binding curve that was fitted to a hyperbolic function of the form:

$$\Delta A_{409} = \frac{\Delta A_{max} * [HA]}{K_d + [HA]} \quad (1)$$

where ΔA_{max} is the maximum absorbance change at 409 nm. The K_d value obtained from the binding curve was found to be in good agreement with the value calculated from k_{off}/k_{on}.

RESULTS AND DISCUSSION

Ferrous L16G AxCP-α and its HA Complex. The UV-vis absorption spectrum of Fe(II) L16G AxCP-α exhibits a Soret maximum at 414 nm with a pronounced 434-nm shoulder (sh), along with weaker bands at 521, 552, and 569 sh (Figure 1). Resonance Raman (RR) spectra obtained with 442 nm laser excitation (near the 434-nm absorbance shoulder) yield porphyrin marker bands at 1350 cm^{-1} (ν_4), 1464 cm^{-1} (ν_3), 1575 cm^{-1} (ν_2), and 1600 cm^{-1} (ν_{10}) (Figure S1, left panel) that are characteristic of five-coordinate (5c) high spin (HS) Fe(II) heme and similar to those of other Fe(II) cytochromes *c′*-α.[28] Changing the excitation wavelength to 407 nm (close to the 414 nm Soret absorbance) leads to a different set of porphyrin marker frequencies at 1354 cm^{-1} (ν_4), 1466 cm^{-1} (ν_3), and 1594 cm^{-1} (ν_2) characteristic of a six-coordinate (6c) Fe(II) heme population (Figure S1, left panel). The low frequency RR region (Figure S1, right panel) also distinguishes two Fe(II) L16G AxCP-α heme populations. Excitation at 442 nm enhances the ν(Fe–His) stretching mode

at 227 cm^{-1} (Figure S1, right panel), which is a characteristic property of 5cHS Fe(II) heme, whereas the disappearance of the ν(Fe–His) mode (Figure S1, right panel) upon switching to 407 nm excitation is consistent with a 6c (rather than 5c) heme. We propose that the 6c heme population in Fe(II) L16G AxCP-α contains a distal H_2O ligand. Although the coordination of H_2O to heme in its Fe(II) redox state is unusual, it is noted that an H_2O ligand is apparent in the crystal structure of Fe(II) L16A AxCP-α.[34] In our previous work, an Fe(III)NO_2^- complex of L16G AxCP-α was converted to an Fe(II)H_2O form as a result of X-ray photoreduction.[35]

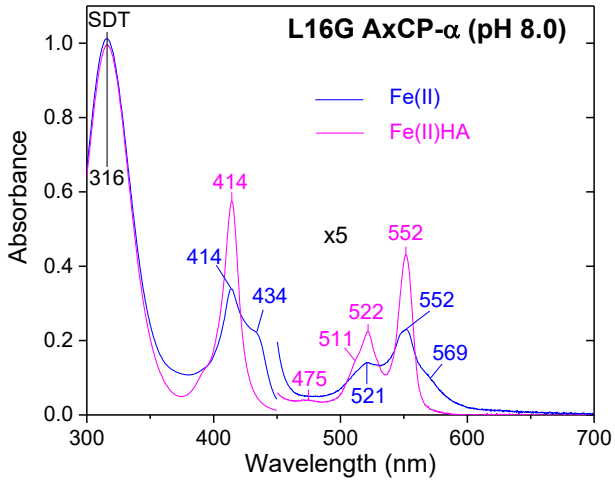

Figure 1. Fe(II) L16G AxCP-α in the presence of 0.1 mM sodium dithionite (SDT) (blue trace) and its Fe(II)HA complex formed upon addition of 14 mM HA (magenta trace).

Table 1. Effect of heme Fe redox state on the absorption and kinetic properties of hydroxylamine (HA) and imidazole (Im) heme complexes of L16G AxCP-α.

L16G complex	λ_{max} (nm)			k_{on} (M^{-1} s^{-1})	k_{off} (s^{-1})	K_d (mM)[a]
Fe(III)HA	409	533	565	4300 ± 300	11 ± 2	2.6 ± 0.5, *(2.4 ± 0.3)*
Fe(II)HA	414	522	552	2880 ± 60	0.0994 ± 0.0003	0.0345 ± 0.0007

Fe(III)Im	413	532	563	1540 ± 30	0.00124 ± 0.00007	0.00081 ± 0.00005
Fe(II)Im	420	525	557	384 ± 7	0.00147 ± 0.00001	0.00383 ± 0.00007

[a] K_d values are calculated from the k_{off}/k_{on} ratio, except for values in parentheses which were determined by titration.

In the presence of excess dithionite, Fe(II) L16G AxCP-α reacts with HA to generate an Fe(II)HA complex (Figure 1, Table 1) characterized by a Soret band at 414 nm and distinctive sharp αβ bands (552 and 522 nm) that resemble those of other 6c Fe(II) heme complexes with non-gaseous axial ligands (Table S1). RR spectra obtained with 407 nm excitation yield porphyrin bands characteristic of a 6c Fe(II) heme complex: ν_4 (1356 cm^{-1}), ν_3 (1491 cm^{-1}), ν_2 (1593 cm^{-1}), and ν_{10} (1620 cm^{-1}), along with a set of low frequency modes (Figure S2). Within the mid-frequency RR region, the predominantly N–O stretching mode of the NH_2OH ligand, ν(N–O), is identified at 906 cm^{-1} from its 17 cm^{-1} downshift with ^{15}N-labeled HA (Figure 2), in good agreement with the predicted value (16 cm^{-1}) approximated by a diatomic N–O oscillator. No other N-isotope sensitive RR bands were observed within the 200 – 1650 cm^{-1} frequency range. By comparison, the Raman spectrum of free aqueous HA in its conjugate base form (NH_2OH) (Figure S3, pH 8.0 spectrum) exhibits a ν(N–O) mode at 916 cm^{-1}, whereas the acidic form of free HA ($^+NH_3OH$) (Figure S3, pH 3.5 spectrum) exhibits an ν(N–O) mode at 1006 cm^{-1}. The fact that the ν(N–O) frequency of the Fe(II)HA complex of L16G AxCP-α differs by only ~10 cm^{-1} from that of free NH_2OH is consistent with previous DFT modeling of the cytochrome *c* nitrite reductase Fe(II)HA complex which suggested that HA behaves only a σ-donor ligand with no additional π-backbonding,[8] with a calculated N–O distance (~1.46 Å) very close to that of free NH_2OH (1.45 Å).[36] A similar conclusion was also reached in earlier studies by Einsle *et al.*[7] Although we were unable to find other RR data for heme-HA complexes in the literature, previous IR measurements

of metal ion NH_2OH complexes (as suspensions in mineral oil) have tentatively assigned ν(N–O) modes within the ~910 – 1035 cm^{-1} region.[37]

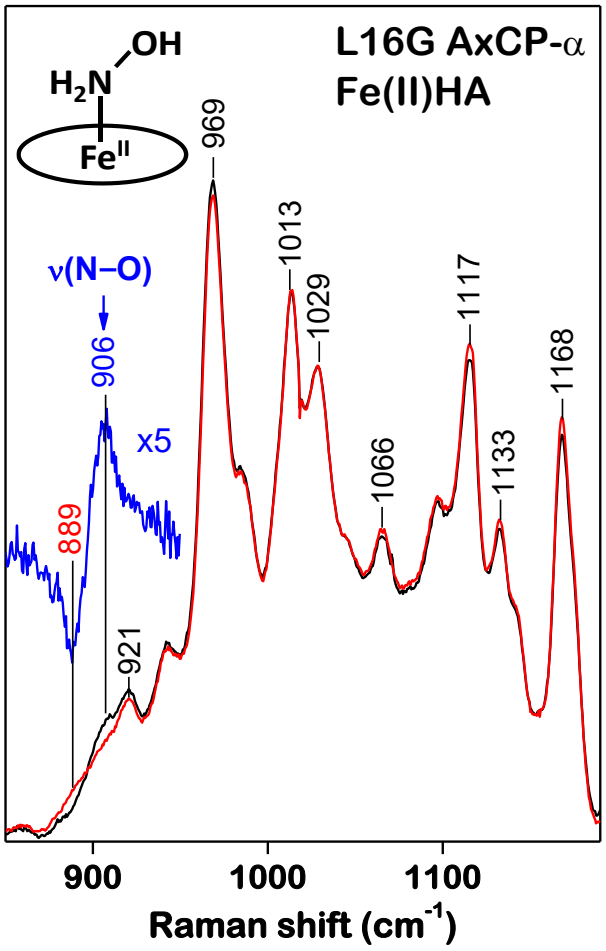

Figure 2. Room-temperature mid-frequency RR spectra of the Fe(II)HA complex of L16G AxCP-α (407 nm excitation) prepared with ^{14}N HA (black trace) and ^{15}N HA (red trace). The ν(N–O) stretching frequency of the HA ligand, highlighted by ^{14}N – ^{15}N difference spectra (blue trace), is observed at 906 cm^{-1}.

UV-vis stopped-flow measurements of the mixing of HA with Fe(II)L16G AxCP-α were used to determine the bimolecular rate constant for Fe(II)HA formation, k_{on}, (2,880 ± 60) M^{-1} s^{-1}, with a *y*-intercept close to zero (Figure 3). Separate ligand replacement measurements (reaction of the

Fe(II)HA complex with CO) were used to determine the off rate constant for Fe(II)HA complex, k_{off}, (0.0994 ± 0.0003) s^{-1} (Figure 4, Table 1). The k_{off}/k_{on} ratio for the Fe(II)HA complex yields the dissociation constant, K_d = 0.0345 ± 0.0007 mM (Table 1). When formed with 0.30 mM HA and 0.1 mM dithionite, the spectroscopic features of the Fe(II)HA complex are stable for ~40 min at room temperature (Figure S4). However, the progressive consumption of dithionite, apparent from the decrease in its 316-nm absorbance band (which does not occur when dithionite is mixed with HA in the absence of protein) suggests that the Fe(II)HA complex undergoes oxidation to the ferric state, which is then reduced rapidly by excess dithionite to regenerate and maintain the Fe(II)HA form. Indeed, upon depletion of the dithionite pool, the Fe(II)HA absorption features are replaced by those of the Fe(III) state (λ_{max} 405 nm) (Figure S4). Over longer timeframes, the Soret maximum decreases in intensity and red shifts to 417 nm, and weaker bands appear at ~540, ~575, and ~630 nm. These absorbance changes resemble those previously observed during the autooxidation of the L16A AxCP-α Fe(II)O_2 complex,[33] and are suggestive of porphyrin degradation due to reactive species (*e.g.* radicals) generated during heme Fe redox chemistry.

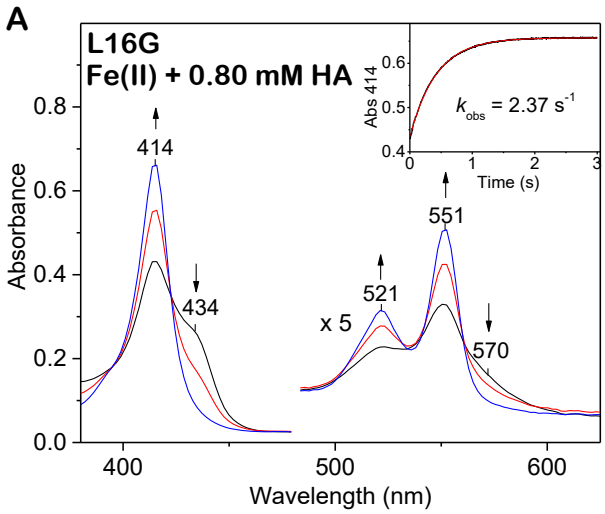

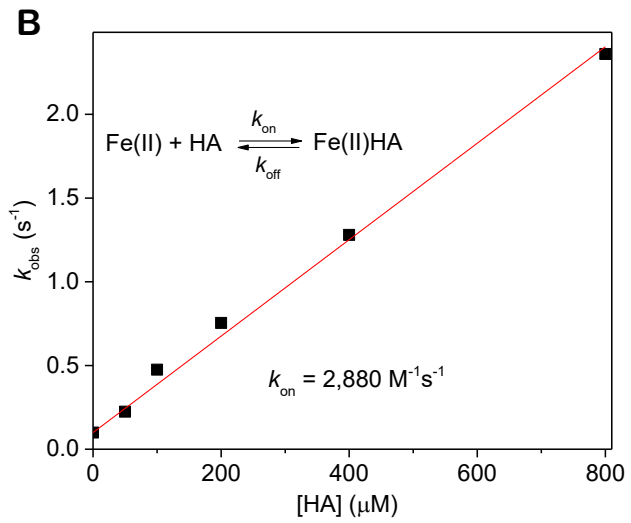

Figure 3. Stopped-flow measurements for the binding of HA to Fe(II) L16G AxCP-α in the presence of 0.14 mM sodium dithionite (pH 8.0). Panel A shows time-resolved absorbance spectra following the mixing of Fe(II) protein with 0.80 mM HA, recorded at 0.002 s (black), 0.3 s (red), and 3.0 s (blue), with a single exponential fit of the 414-nm time course (inset, red trace) yielding a pseudo first order rate constant, k_{obs}. The bimolecular rate constant for Fe(II)HA formation, k_{on} (2880 ± 60) M^{-1} s^{-1} was obtained from the slope of a k_{obs} vs [HA] plot (Panel B), with the *y*-intercept fixed at the value of k_{off} (0.0994 s^{-1}) determined in separate experiments (see Figure 4).

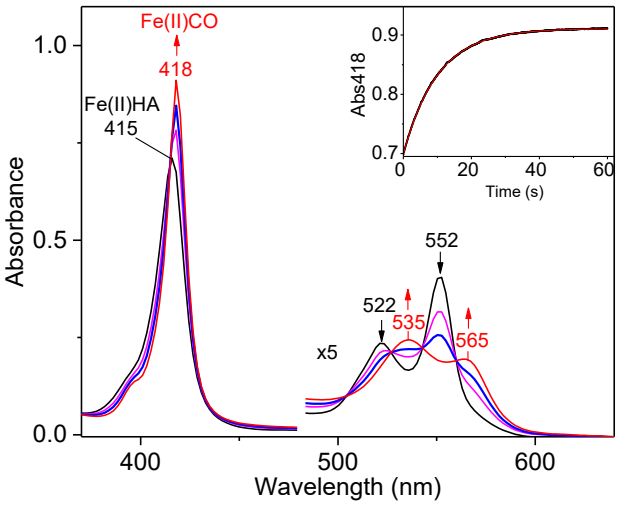

Figure 4. Stopped-flow measurements for the release of HA from the L16G AxCP-α Fe(II)HA complex (pH 8.0). Upon mixing the Fe(II)HA complex (λ_{max} 415, 522, 552 nm) with 0.5 mM CO, time-resolved spectra recorded at 0.002 s (black trace), 5.0 s (magenta trace), 12 s blue trace), and 60 s (red trace) show conversion to the Fe(II)CO state (λ_{max} 418, 535, 565 nm), with the rate constant for HA release (k_{off}) as the rate determining step. The value of k_{off} (0.0994 s^{-1}) was obtained from a single exponential fit of the 418 nm course (inset, red trace).

Previous studies of Fe(II) containing globins (from animals, cyanobacteria and plants) have shown that HA oxidizes the heme center to Fe(III) to form ammonium, with an overall HA:heme:NH_4^+ stoichiometry of 1:2:1.[11,24,25] Although the mechanism for the two electron reduction of HA remains unclear, it was proposed that oxidation of the Fe(II) heme occurs via a short-lived (and undetectable) Fe(II)HA intermediate. Indeed, following a distal pocket His73→Leu replacement in rice phytoglobin, stopped flow measurements detected a transient species with absorption features consistent with an Fe(II)HA complex and kinetic parameters of k_{on} = 4.2 × 10^5 M^{-1} s^{-1} and k_{off} = 190 s^{-1}, corresponding to K_d value of 0.45 mM (Table S2).[24] To our knowledge, the transient Fe(II)HA species observed in H73L rice phytoglobin is the only other detectable Fe(II)HA heme protein species characterized to date. Whereas the k_{on} value for H73L rice phytoglobin (420,000 M^{-1} s^{-1}) is two orders of magnitude higher than that of the L16G AxCP-α complex (2,880 M^{-1} s^{-1}), the phytoglobin k_{off} value (190 s^{-1}) is *three* orders of magnitude higher compared to L16G AxCP-α (0.0994 s^{-1}) (Table S1). Consequently, L16G AxCP-α exhibits a lower K_d value than that of the phytoglobin variant (0.035 vs 0.45 mM), corresponding to a ~13-fold higher HA affinity. Although the structural basis for these differences remains to be established, the higher k_{on} for H73L phytoglobin points to a more accessible heme site, whereas the lower k_{off}

value of L16G AxCP-α might arise from more efficient geminate recombination (a property exhibited by gas complexes of the related L16A variant).[38]

Ferric L16G AxCP-α and its HA Complex. To our knowledge, there have been no previous reports of heme proteins characterized in both their Fe(II)HA and Fe(III)HA states. In order to probe the influence of the Fe redox state on heme-HA coordination, we compared the properties of Fe(II)HA complex of L16G AxCP-α (*vide supra*) with those of its Fe(III)HA species. The Fe(III) redox state of L16G AxCP-α exhibits a Soret absorption maximum at 405 nm, together with weaker bands at 498 and 627 nm.[35] Recent RR studies of Fe(III) L16G AxCP-α have revealed a single 6cHS heme population.[35] consistent with the presence of a distal water ligand. Our current stopped-flow UV-vis absorption measurements show that Fe(III) L16G AxCP-α (λ_{max} 405, 498, 627 nm) reacts with HA to generate an Fe(III)HA complex (λ_{max} 409, 529, 562sh nm) with absorbance bands similar to those reported for other Fe(III)HA heme protein complexes (Figure 5, Table 1 and S1). Kinetic time courses at 409 nm, recorded over 0.2 s for a range of HA concentrations (0.6 – 15 mM) (Figure 5B), were used to determine the bimolecular rate constant for Fe(III)HA formation, k_{on}, (4,300 ± 300) M^{-1} s^{-1}, together with the off rate constant, k_{off}, (11 ± 2) s^{-1} (Figure 5C, Table 1). The K_d value (2.6 ± 0.5) mM of the Fe(III)HA L16G-α complex, calculated from the k_{off}/k_{on} ratio is in good agreement with that determined from titration (2.4 ± 0.3) mM by analyzing the magnitude of stopped-flow absorbance changes for Fe(III)HA formation (ΔA_{409}) as a function of HA concentration (Figure 5D, Table 1). Overall, the affinity of the L16G AxCP-α Fe(III)HA complex (K_d ~ 2.5 mM) is within the range of values reported for other Fe(III)HA heme proteins (K_d ~ 1 – 18 mM)(Table S2).[1,13,14,16-18]

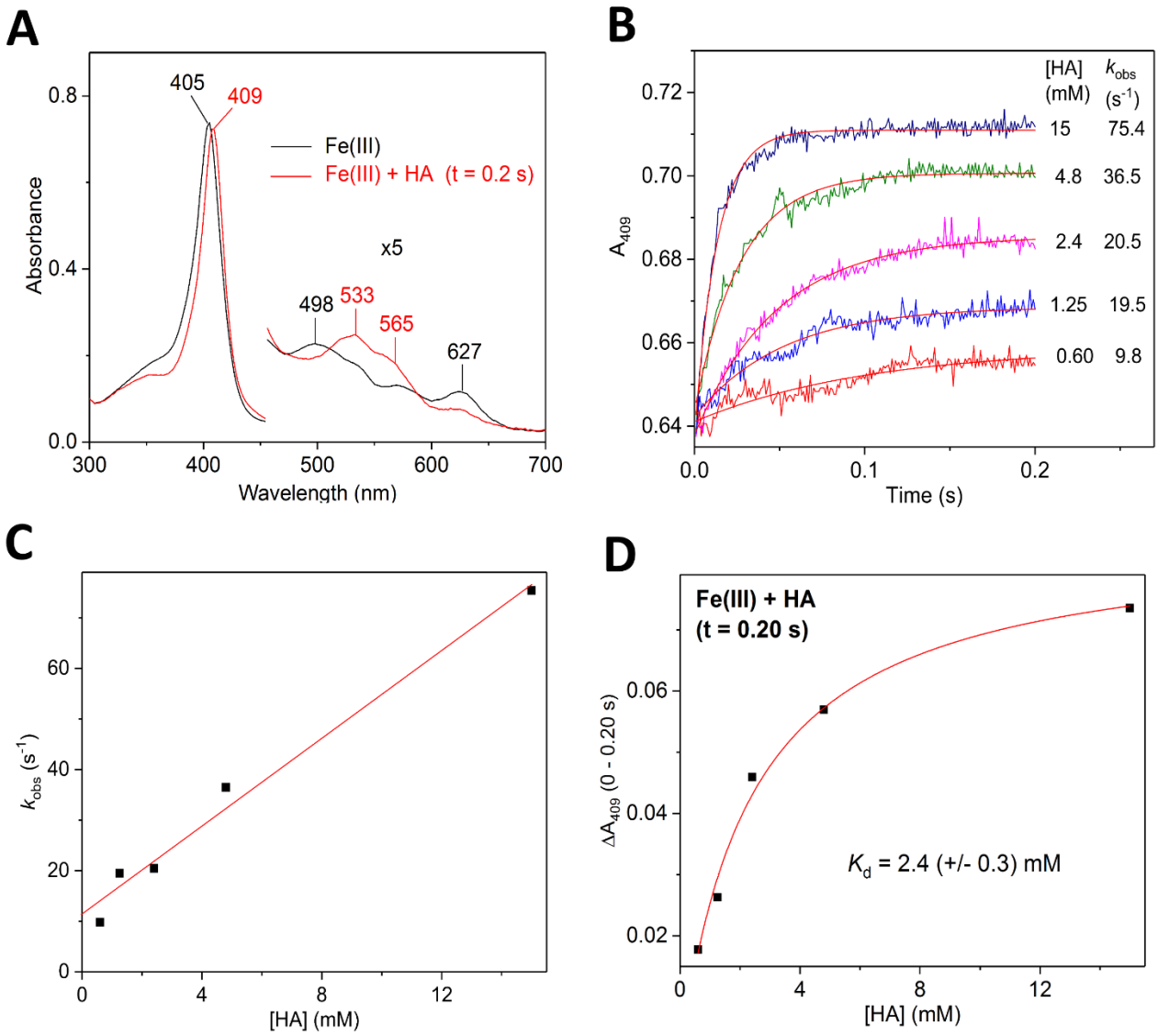

Figure 5. Stopped-flow measurements for the reaction of HA with Fe(III) L16G AxCP-α (pH 8.0). Panel A shows UV-visible absorbance spectra of Fe(III) L16G AxCP-α (black trace) and the Fe(III)HA product recorded 0.2 s after mixing with 15 mM HA (red trace). Kinetic time courses

at 409 nm, obtained for a range of HA concentrations (0.6 – 15 mM) (panel B), were each fitted to a single exponential function to yield a pseudo rate constants, k_{obs}. The bimolecular rate constant for Fe(III)HA formation, k_{on} (4,300 ± 300) M^{-1} s^{-1} was obtained from the slope of a k_{obs} vs [HA] plot, with the *y*-intercept yielding the rate constant for HA release, k_{off} (11 ± 2) s^{-1} (panel C). The ratio of k_{off}/k_{on} yields a value for the dissociation constant, K_d (2.6 ± 0.5) mM. The K_d value for the Fe(III)HA complex was also determined by titration. In this case, a plot of the change in absorbance at 409 nm (ΔA409) vs HA concentration for each stopped-flow time course was fitted to a hyperbolic function (panel D), yielding a value of K_d (2.4 ± 0.3) mM in good agreement with the above value calculated from k_{off}/k_{on}.

Subsequent to its formation, the Fe(III)HA complex appears to undergo partial reduction to the Fe(II)HA state, as evidenced by the appearance of new absorption bands at ~413, ~522, and ~552 nm (Figure S5) reminiscent of the Fe(II)HA complex (Figure 1)(Table 1). The Fe(II)HA absorption features reach a maximum intensity after ~ 5 mins, after which additional absorption changes occur that are similar to the aging of the oxidized Fe(II)HA sample (*vide supra*)(Figure S4), and which are attributed to heme degradation (*vide supra*). Unlike the Fe(II)HA complex, whose lifetime could be prolonged by the presence of excess reductant (dithionite) (*vide supra*), we were unable to inhibit the redox-associated decay of the Fe(III)HA species by the addition of excess oxidant (ferricyanide), since this resulted in the consumption of free HA. Although the mechanism of Fe(III)HA → Fe(II)HA redox conversion in L16G AxCP-α remains to be elucidated, many Fe(III) porphyrins react with HA to form the Fe(II) state along with various HA disproportion products (including NO, N_2O, N_2, or NH_4^+), with a range of redox reactions proposed.[19-22] We note that among heme proteins known to form stable Fe(III)HA complexes (Table S2), those of cytochromes P460 have particularly low Fe(III)/(II) reduction potentials (E^o

= -400 and -428 mV for NeP460 and AL212P460, respectively).[21] The redox chemistry of L16G AxCP-α heme-HA complexes will be the subject of future investigations in this laboratory.

Influence of the Fe Redox State on Heme-HA Affinity of L16G AxCP-α. Our characterization of both the Fe(II)HA and Fe(III)HA complexes of L16G AxCP-α reveals the extent to which its heme Fe redox state influences reversible HA binding. Notably, the HA affinity of the L16G AxCP-α Fe(II)HA complex is ~70-fold higher than that of its Fe(III)HA counterpart, as reflected in K_d values of 0.0345 mM and ~2.5 mM, respectively (Table 1). Whereas the k_{on} values for the Fe(II)HA (2,880 M^{-1} s^{-1}) and Fe(III)HA (4,300 M^{-1} s^{-1}) complexes are quite similar, the k_{off} value of the Fe(II)HA species (0.0994 s^{-1}) is significantly lower than that of its Fe(III)HA counterpart (11 s^{-1}), which accounts for the higher HA affinity of the Fe(II) state. Previous DFT calculations for HA binding to cytochrome *c* nitrite reductase showed no evidence of π-backbonding interactions that might boost the HA affinity of the Fe(II)HA complexes relative to Fe(III)HA.[7,8] Indeed, our Raman data show that the N–O bond of NH_2OH is relatively unperturbed by coordination to Fe(II) L16G AxCP-α (*vide supra*), which argues against π-backbonding as the reason for increased HA affinity. On the other hand, we note that L16G and L16A AxCP-α variants exhibit unusually low k_{off} values for their Fe(II)XO complexes (X = C, N, O).[32,33] Further studies of the L16A variant have shown that sluggish ligand release arises from ultra-efficient geminate recombination, ascribed to the conformation of the 7-propionate heme substituent which blocks ligand escape from the distal heme pocket.[38] If propionate conformations were to vary between the Fe(II) and Fe(III) states, this could provide a redox-based determinant of ligand off rates (including for HA) in L16A(G) variants of AxCP-α. Future comparative of heme-HA complexes should shed more light on the influence of heme redox state and heme pocket environment on heme-HA bonding.

Imidazole Complexes of L16G AxCP-α: Gauging the Influence of the Fe Redox State on the Heme-HA Affinity of Other Proteins. A key finding of the present study is that the HA affinity of Fe(II) L16G AxCP-α (K_d = 0.0345 mM) is ~70-fold higher than its Fe(III) counterpart (K_d ~2.5 mM), due mainly to the Fe(II)HA complex having a lower k_{off} (0.0994 s^{-1}) than the Fe(II)HA complex (11 s^{-1}) (Table 1). This finding raises the question: do other heme proteins also exhibit higher HA affinity in the Fe(II) state? However, since reported K_d values for other heme-HA complexes are exclusively for either the Fe(III) [13,14,16-18] or Fe(II) state,[24] the extent to which Fe redox state controls HA affinities in other heme proteins is not known. As a means of predicting redox-based HA reactivity trends in other proteins, we characterized L16G AxCP-α complexes with imidazole (Im) – a non-redox ionizable ligand (pK_a 7.0) for which binding data are available for both the Fe(III) and Fe(II) redox states of several heme proteins (Table S2).[37-40] We reasoned that by comparing the influence of the Fe redox state on heme-Im affinities in L16G and other proteins (via the Fe(II)Im/Fe(III)Im K_d ratios), we could then correlate the redox-dependent HA affinities of L16G with likely values for other heme proteins.

The K_d values of both the Fe(II)Im and Fe(III)Im complexes of L16G AxCP-α were calculated from k_{off}/k_{on} ratios determined from kinetic measurements (since affinities were too high for accurate determination by titration). In its Fe(II) state, L16G AxCP-α forms an Fe(II)Im complex (λ_{max} 420, 525, 557 nm) (Figure S6) with absorption bands red shifted by ~3 – 5 nm relative to those of the Fe(II)HA complex (Table 1). Using stopped-flow measurements, the bimolecular rate constant for Fe(II)Im formation was determined (k_{on} = 384 ± 7 M^{-1} s^{-1}) (Figure S6, Table 1). Ligand replacement measurements of the reaction of the Fe(II)HA complex with CO, enabled the determination of the off rate constant for Fe(II)HA complex, (k_{off} = 0.0994 ± 0.0003 s^{-1}) (Figure S7, Table 1). By means of the k_{off}/k_{on} ratio, the K_d value of the Fe(II)Im complex was calculated

as 0.00383 mM (Table 1). The Fe(III)Im counterpart of L16G AxCP-α exhibits absorption features (λ_{max} 413, 532, 563 nm)(Figure S8A) that are somewhat reminiscent of its Fe(III)HA complex (Figure 1A), but with the Soret band red-shifted by 4 nm (Table 1). Stopped-flow measurements were used to determine the bimolecular rate constant for Im binding to the Fe(III) state (k_{on} = 1,540 ± 30 M^{-1} s^{-1}) (Figure S8, Table 1). The k_{off} value for the Fe(III)Im complex was determined using separate ligand replacement experiments with NO (Figure S9). In the presence of NO, the Fe(III)Im complex converts to a predominant Fe(III)NO species (λ_{max} 418, 536, 567 nm) over a period of ~30 mins (Figure S9), with reductive nitrosylation to the Fe(II)NO state (λ_{max} 416, 541, 572 nm) occurring over a period of ~160 min. The absorption features of both heme-nitrosyl species resemble those previously reported.[35] A double exponential fit of the kinetic time course yields the value of k_{off} (0.00124 ± 0.0007 s^{-1}) as the rate constant for Fe(III)Im → Fe(III)NO conversion, with a rate constant, k_{rn} = 5.5 (± 0.6) x 10^{-4} s^{-1} for the slower reductive nitrosylation phase (Figure S7, Table 1). From the k_{off}/k_{on} ratio, the K_d value of the Fe(III)Im complex was calculated as 0.00081 mM (Table 1).

L16G AxCP-α exhibits an unusually high affinity for Im relative to other heme proteins. For example, the K_d value of the Fe(III)Im complex (0.00081 mM), calculated from the k_{off}/k_{on} ratio (Table 1), shows that Im affinity of Fe(III) L16G AxCP-α is *four* orders of magnitude higher than that of Fe(III) Mb (K_d ~ 20 mM) (Table S2).[37,38] This difference is even more pronounced in the reduced state, for which Fe(II)Im K_d values for L16G AxCP-α (0.0038 mM) and Mb (1500 mM)[39] reveal a *five* order of magnitude higher Im affinity for L16G AxCP-α (Table S2). Redox-dependent trends in heme-Im affinities provide a means of gauging the (likely) influence of the Fe redox state on heme-HA affinities. Data available for other heme proteins show that the heme-Im affinity of the Fe(II) state is significantly lower than that of the Fe(III) state, as reflected in the

Fe(II)Im/Fe(III)Im K_d ratios for Mb (~ 68), Hb (~ 225), and cytochrome *c* (~ 14) (Table S2).[39-42] However, in the case of L16G AxCP-α, the heme-Im affinity of the Fe(II) state (K_d = 0.00383 mM) is much closer to that of the Fe(III) state (K_d = 0.00081 mM) (Table 1 and S1), corresponding to a Fe(III)Im/Fe(II)Im K_d ratio of 4.7. In other words, the L16G AxCP-α heme pocket appears to elevate the Fe(III)Im/Fe(II)Im K_d ratio by a factor of ~3 – 50 relative to other heme proteins. If we assume that the L16G AxCP-α heme pocket also boosts the Fe(III)HA/Fe(II)HA K_d ratio by a similar amount (factor of ~3 – 50) relative to other heme proteins, then the observed Fe(III)HA/Fe(II)HA K_d ratio of ~70 for L16G AxCP-α suggests that the Fe(II)HA complexes of other heme proteins (which have remained essentially uncharacterized to date) may have HA affinities close to those of their Fe(III)HA counterparts.

SUMMARY AND CONCLUSIONS

Complexes of HA with Fe(III) and/or Fe(II) active sites of microbial heme proteins are important intermediates in the biogeochemical nitrogen cycle. In order to shed light on fundamental aspects of heme-HA coordination chemistry (including the effect of Fe redox state on kinetic and spectroscopic properties), we characterized reversible HA binding to L16G AxCP-α, a microbial heme protein that exhibits enhanced affinity for exogenous ligands. The Fe(II)HA complex of L16G AxCP-α exhibits sharply-defined αβ absorption bands near 550 and 520 nm, and an NH_2OH ligand ν(N–O) RR mode at 906 cm^{-1} (the first such vibration reported for heme-bound HA). These spectroscopic benchmarks for the Fe(II)HA species provide a foundation for future characterization of heme-HA reaction mechanisms. A key finding from the present study is that the heme-HA affinity of L16G AxCP-α is ~70-fold higher in the Fe(II) state (K_d = 0.0345 mM)

than in the Fe(III) state (K_d ~ 2.5 mM), due primarily to the Fe(II)HA species having a lower k_{off} value (0.0994 s^{-1} vs 11 s^{-1}). Moreover, a comparison of K_d values for HA and imidazole complexes suggests that in general, Fe(II) heme cofactors have HA affinities similar to those of their Fe(III) counterparts. Accordingly, from the standpoint of substrate affinity, both Fe(II)HA and Fe(III)HA species should be considered in mechanisms of HA metabolism. Although heme-HA complexes of L16G AxCP-α ultimately exhibited redox-based decomposition, we found that the Fe(II)HA state was stabilized in the presence of excess dithionite. We suggest that a similar approach could be applied to stabilize the Fe(II)HA complexes of other heme proteins, which to date have remained elusive.

ASSOCIATED CONTENT

Supporting Information. The following files are available free of charge.

Additional kinetic and spectroscopic data (PDF)

AUTHOR INFORMATION

Corresponding Author

*E-mail: candrew@eou.edu

Present Addresses

[‖]Division of Biology and Chemistry, Paul Scherer Institut, 5232 Villigen, Switzerland

Author Contributions

The manuscript was written through contributions of all authors. All authors have given approval to the final version of the manuscript.

Notes

The authors declare no competing financial interest.

ACKNOWLEDGMENTS

This work was supported by the National Science Foundation (MCB-1411963 and MCB-1921670 grants to C. R. A.). We also acknowledge ASTEO scholarship support from the National Science Foundation to Quentin Durfee (S-STEM 1458165). The authors thank Dr. Pierre Moënne-Loccoz (School of Medicine, Oregon Health & Science University) for assistance with resonance Raman measurements, and Professor Samar Hasnain's Molecular Biophysics Group at the University of Liverpool UK for original plasmid construction of the L16G AxCP-α variant.

REFERENCES

(1) Caranto, J. D.; Vilbert, A. C.; Lancaster, K. M., *Nitrosomonas europaea* cytochrome P460 is a direct link between nitrification and nitrous oxide emission. *Proc. Natl. Acad. Sci. USA* **2016**, *113*, 14704–14709.

(2) Lehnert, N.; Dong, H. T.; Harland, J. B.; Hunt, A. P.; White, C. J., Reversing nitrogen fixation. Nat. Rev. Chem. **2018**, *2*, 278–289.

(3) Ensign, S. A.; Hyman, M. R.; Arp, D. J., *In vitro* activation of ammonia monooxygenase from *Nitrosomonas europaea* by copper. *J. Bacteriol.* **1993**, *175*, 1971–1980.

(4) Hanson, R. S.; Hanson, T. E., Methanotrophic bacteria. *Microb. Rev.* **1996**, *60*, 439–471.

(5) Nyerges, G.; Stein, L. Y., Ammonia cometabolism and product inhibition vary considerably among species of methanotrophic bacteria. *FEMS Microbiol. Lett.* **2009**, *297*, 131–136.

(6) Vilbert, A. C.; Caranto, J. D.; Lancaster, K. L., Influences of the heme-lysine crosslink in cytochrome P460 over redox catalysis and nitric oxide sensitivity. *Chem. Sci.* **2018**, *9*, 368–379.

(7) Einsle, O.; Messerschmidt, A.; Huber, R.; Kroneck, P. M. H.; Neese, F., Mechanism of the six-electron reduction of nitrite to ammonia by cytochrome *c* nitrite reductase. *J. Am. Chem. Soc.* **2002**, *124*, 11737–11745.

(8) Bykov, D.; Plog, M.; Neese, F., Heme-bound nitroxyl, hydroxylamine, and ammonia ligands as intermediates in the reaction cycle of cytochrome *c* nitrite reductase: a theoretical study. *J. Inorg. Biochem.* **2014**, *19*, 97–112.

(9) Kern, M.; Volz, J.; Simon, J., The oxidative and nitrosative stress defense network of *Wollinella succinogenes*: cytochrome *c* nitrite reductase mediates the stress response to nitrite, nitric oxide, hydroxylamine and hydrogen peroxide. *Environ. Microbiol.* **2011**, *13*, 2478–2494.

(10) Igamberdiev, A. U.; Hill, R. D., Nitrate, NO and haemoglobin in plant adaptation to hypoxia: an alternative to classic fermentation pathways. *J. Expt. Bot.* **2004**, *55*, 2473–2482.

(11) Sturms, R.; DiSpirito, A. A.; Fulton, B.; Hargrove, M. S. Hydroxylamine reduction to ammonium by plant and cyanobacterial hemoglobins. *Biochemistry*, **2011**, *50*, 10829–10835.

(12) Robinson, R. A.; Bower, V. E., The ionization constant of hydroxylamine. *J. Phys. Chem.* **1961**, *65*, 1279–1280.

(13) Sakamoto, H.; Higashimoto, Y.; Hayashi, S.; Sugishima, M.; Fukuyama, K.; Palmer, G.; Noguchi, M., Hydroxylamine and hydrazine bind directly to the heme iron of the heme-heme oxygenase-1 complex. *J. Inorg. Biochem.* **2004**, *98*, 1223–1228.

(14) Wariishi, H.; Nonaka, D.; Johjima, T.; Nakamura, N.; Naruta, Y.; Kubo, S.; Fukuyama, K., Direct binding of hydroxylamine to the heme iron of *Arthromyces ramosus* peroxidase. Substrate analogue that inhibits compound I formation in a competetive manner. *J. Biol. Chem.* **2000**, *275*, 32919–32924.

(15) Fukuyama, K.; Okada, O., Structures of cyanide, nitric oxide and hydroxylamine complexes of *Arthromyces ramosus* peroxidase at 100 K refined to 1.3 Å resolution: coordination geometries of the ligands to the haem iron. *Acta Crystallogr Sect D: Biol Crystallogr.* **2007**, *63*, 472–477.

(16) Marques, M. M.; Munro, O. Q.; Munro, T.; de Wet, M.; Vashi, P. R., Coordination of N-donor ligands by the monomeric ferric porphyrin N-Acetylmicroperoxidase-8. *Inorg. Chem.* **1999**, *38*, 2312-2319.

(17) Smith, M. A.; Majer, S. H.; Vilbert, A. C.; Lancaster, K. M., Controlling a burn: outer-sphere gating of hydroxylamine oxidation by a distal base in cytochrome P460. *Chem. Sci.* **2019**, *10*, 3756–3764.

(18) Coleman, R. E.; Vilbert, A. C.; Lancaster, K. M., The heme-Lys cross-link in cytochrome P460 promotes catalysis by enforcing secondary coordination sphere architecture. *Biochemistry* **2020**, Article ASAP DOI: 10.1021/acs.biochem.0c00261

(19) Feng, D.; Ryan, M. D., Electrochemistry of nitrite reductase model compounds. 3. Formation and characterization of a bis(hydroxylamine)(tetraphenylporphyrinato)iron(II) complex. *Inorg. Chem.* **1987**, *26*, 2480–2483.

(20) Choi, I.-K.; Liu, Y.; Wei, Z.; Ryan, M. D., Reactions of hydroxylamine with metal porphyrins. *Inorg. Chem.* **1997**, *36*, 3113–3118.

(21) Bari, S. E.; Amorebieta, V. T.; Gutierrez, M. M.; Olabe, J. A.; Doctorovich, F., Disproportionation of hydroxylamine by water-soluble iron(III) porphyrinate compounds. *J. Inorg. Biochem.* **2010**, *104*, 30–36.

(22) Bazylinski, D. A.; Arkowitz, R. A.; Hollocher, T. C., Decomposition of hydroxylamine by hemoglobin. *Arch. Biochem. Biophys.*, **1987**, *259*, 520–526.

(23) McQuarters, A. B.; Goodrich, L. E.; Goodrich, C. M.; Lehnert, N., Disproportionation of *O*-benzylhydroxylamine catalyzed by a ferric *bis*-picket fence porphyrin complex, **2013**, *639*, 1520–1526.

(24) Athwal, N. S.; Alagurajan, J.; Andreotti, A. H.; Hargrove, M. S., Role of reversible histidine coordination in hydroxylamine reduction by plant hemoglobins (phytoglobins). *Biochemistry*, **2016**, *55*, 5809–5817.

(25) Ascenzi, P.; Ciacco, C.; Gasperi, T.; Pesce, A.; Caporaso, L.; Coletta, M., Hydroxylamine-induced oxidation of ferrous carbonylated truncated hemoglobins from *Mycobacterium tuberculosis* and *Campylobacter jejuni* is limited by carbon monoxide dissociation. *J. Biol. Inorg.* Chem., **2017**, *22*, 977–986.

(26) Rahman, M. H; Ryan, M. D., Redox and spectroscopic properties of iron porphyrin nitroxyl in the presence of weak acids. *Inorg. Chem.*, **2017**, *56*, 3302–3309.

(27) Rahman, M. H; Ryan, M. D., Insight into solvent coordination of an iron porphyrin hydroxylamine complex from spectroscopy and DFT calculations. *Eur. J. Inorg. Chem.* **2018**, *16*, 1762–1765.

(28) Hough, M. A.; Andrew, C. R., Cytochromes *c′*: Structure, reactivity and relevance to haem-based gas sensing. In *Advances in Microbial Physiology. Recent advances in microbial oxygen-binding proteins*, Poole, R. K., Ed. Elsevier: UK, **2015**; Vol. 67, pp 1–84.

(29) Bergmann, D. J.; Zahn, J. A.; DiSpirito, A. A., Primary structure of cytochrome *c′* of *Methylococcus capsulatus* Bath: evidence of a phylogenetic link between P460 and *c′*-type cytochromes. *Arch. Microbiol.* **2000**, *173*, 29–34.

(30) Elmore, B. O.; Bergmann, D. J.; Klotz, M. G.; Hooper, A. B., Cytochromes P460 and *c′*-beta; a new family of high-spin cytochromes *c*. *FEBS Lett.* **2007**, *581*, 911–916.

(31) Adams, H. R.; Krewson, C.; Vardanega, J. E.; Fujii, S.; Moreno-Chicano, T.; Sambongi, Y.; Svistunenko, D.; Paps, J.; Andrew, C. R.; Hough, M. A., One fold, two functions: cytochrome P460 and cytochrome *c′*-β from the methanotroph *Methylococcus capsulatus* (Bath). *Chem. Sci.* **2019**, *10*, 3031–3041.

(32) Antonyuk, S. V.; Rustage, N.; Petersen, C. A.; Arnst, J. L.; Heyes, D. J.; Sharma, R.; Berry, N. G.; Scrutton, N. S.; Eady, R. R.; Andrew, C. R.; Hasnain, S. S., Carbon monoxide poisoning is prevented by the energy costs of conformational changes in gas-binding haemproteins. *Proc. Natl. Acad. Sci. USA* **2011**, *108*, 15780–15785.

(33) Garton, E. M.; Pixton, D. A.; Petersen, C. A.; Eady, R. R.; S., H. S.; Andrew, C. R., A distal pocket Leu residue inhibits the binding of O_2 and NO at the distal heme site of cytochrome *c′*. *J. Am. Chem. Soc.* **2012**, *134*, 1461–1463.

(34) Kekilli, D.; Petersen, C. A.; Pixton, D. A.; Ghafoor, D. D.; Abdullah, G. H.; Dworkowski, F. S. N.; Wilson, M. T.; Heyes, D. J.; Hardman, S. J. O.; Murphy, L. M.; Strange, R. W.; Scrutton, N. S.; Andrew, C. R.; Hough, M. A., Engineering proximal vs. distal heme–NO coordination via dinitrosyl dynamics: implications for NO sensor design. *Chem. Sci.* **2017**, *8*, 1986–1994.

(35) Nilsson, Z. N.; Mandella, B. L.; Sen, K.; Kekilli, D.; Hough, M. A.; Moënne-Loccoz, P.; Andrew, C. R., Distinguishing nitro vs nitrito coordination in cytochrome *c′* using vibrational spectroscopy and density functional theory. *Inorg. Chem.* **2017**, *56*, 13205–13213.

(36) Shi, K.-L.; Wang, R.Q., On the N–O bond length in free and *N*-protonated hydroxylamine, and redetermination of the crystal structure of hydroxylammonium chloride, $(H_3NOH)Cl$. *J. Mol. Struct.* **1987**, *160*, 109–116.

(37) Kharitonov, Y. Y.; Sarakhov, M. A.; Baranovskii, I. B.; Ikramov, K. U., Vibrational frequencies of coordinated hydroxylamine. *Opt. Spectrosk.*, **1965**, *19*, 460–461.

(38) Andrew, C. R.; Petrova, O. N.; Lamarre, I.; Lambry, J.-C.; Rappaport, F.; Negrerie, M., The dynamics behind the affinity: Controlling heme-gas affinity *via* geminate recombination and heme propionate conformation in the NO carrier cytochrome *c′*. *ACS Chem. Biol.* **2016**, *11*, 3191–3201.

(39) Mansy, S. S.; Olson, J. S.; Gonzalez, G.; Gilles-Gonzalez, M. A., Imidazole is a sensitive probe of steric hindrance in the distal pockets of oxygen-binding heme proteins. *Biochemistry* **1998**, *37*, 12452–12457.

(40) Diven, W. F.; Goldsack, D. E.; Alberty, R. A., Temperature jump kinetic studies of the binding of imidazole by sperm whale myoglobin. *J. Biol. Chem.* **1965**, *240*, 2437–2441.

(41) Antonini, E.; Brunori, M., in Hemoglobin and Myoglobin in their Reactions with Ligands, Neuberger, A.; Tatum, E. L., Eds. North-Holland Publishing Co., Amsterdam, 1971.

(42) Viola, F.; Aime, S.; Coletta, M.; Desideri, A.; Fasano, M.; Paoletti, S.; Tarricone, C.; Ascenzi, P., Azide, cyanide, fluoride, imidazole and pyridine binding to ferric and ferrous native horse heart cytochrome *c* and to its carboxymethylated derivative: a comparative study. *J. Inorg. Biochem.* **1996**, *62*, 213–222.

For Table of Contents Only

Table of Contents Graphic

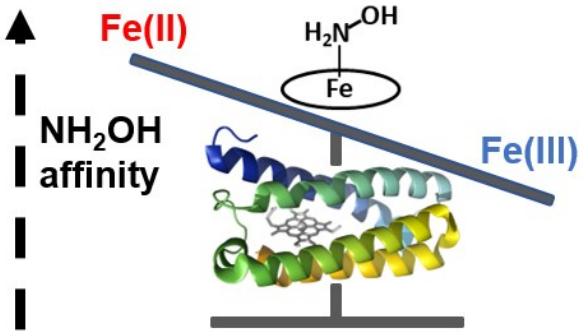

Synopsis

Hydroxylamine (NH_2OH) reactivity with a *c*-type cytochrome has been characterized with the heme in its Fe(III) and Fe(II) states. Time-resolved UV-visible absorption measurements highlight the influence of the iron redox state on heme-hydroxylamine affinity and dynamics. Resonance Raman spectroscopic measurements also identify the stretching vibration of the N–O bond within the NH_2OH ligand.